IOP PUBLISHING JOURNAL OF NEURAL ENGINEERING

J. Neural Eng. **6** (2009) 036001 (15pp) doi:10.1088/1741-2560/6/3/036001

Force estimation from ensembles of Golgi tendon organs

M P Mileusnic and G E Loeb

Department of Biomedical Engineering, Alfred E. Mann Institute for Biomedical Engineering, University of Southern California, Los Angeles, CA, USA

E-mail: gloeb@usc.edu

Received 24 October 2008
Accepted for publication 13 March 2009
Published 14 April 2009
Online at stacks.iop.org/JNE/6/036001

Abstract

Golgi tendon organs (GTOs) located in the skeletal muscles provide the central nervous system with information about muscle tension. The ensemble firing of all GTO receptors in the muscle has been hypothesized to represent a reliable measure of the whole muscle force but the precision and accuracy of that information are largely unknown because it is impossible to record activity simultaneously from all GTOs in a muscle. In this study, we combined a new mathematical model of force sampling and transduction in individual GTOs with various models of motor unit (MU) organization and recruitment simulating various normal, pathological and neural prosthetic conditions. Our study suggests that in the intact muscle the ensemble GTO activity accurately encodes force information according to a nonlinear, monotonic relationship that has its steepest slope for low force levels and tends to saturate at the highest force levels. The relationship between the aggregate GTO activity and whole muscle tension under some pathological conditions is similar to one seen in the intact muscle during rapidly modulated, phasic excitation of the motor pool (typical for many natural movements) but quite different when the muscle is activated slowly or held at a given force level. Substantial deviations were also observed during simulated functional electrical stimulation.

1. Introduction

The Golgi tendon organ (GTO) is a specialized mechanoreceptor that is found in most mammalian skeletal muscles. It lies in series between small groups of muscle fibers and their tendon or aponeurosis of origin or insertion (Golgi 1878, 1880) (figure 1). Typically, tens of GTOs are distributed unevenly across the myotendinous junction, most densely inhabiting the deep areas of the muscle (muscle core), which in heterogeneous muscles is the area rich in slow muscle fibers (Lund *et al* 1978, Richmond and Stuart 1985, Swett and Eldred 1960). Individual GTOs respond vigorously to active tension produced by those muscle fibers that insert into their capsules. The relationship between this afferent activity and whole muscle tension remains controversial, as does the role of this force feedback in motor control and motor learning (Jones 1986).

This study builds on a recent comprehensive review of the structure and function of an individual GTO that provides a mathematical model that accounts well for its transduction properties as described in the literature (Mileusnic and Loeb 2006). Only the most salient facts are summarized here. The typical GTO is linked mechanically to about 3–50 muscle fibers belonging to numerous motor units (MUs) (Jami 1992). The structure of the GTO is composed largely of the myotendinous collagen from each muscle fiber, which is distributed into a dense outer capsule and a loosely packed inner core. A single myelinated afferent axon enters the GTO near its equator and passes into the core, where it bifurcates into primary branches extending proximally and distally in the core (figure 1(b)). These branch further, producing a large network of unmyelinated sensory endings that are intertwined among the loosely packed collagen. Tension in a given muscle fiber results in mechanical distortion and depolarization of these transduction zones. Action potentials can be initiated from at least two independent sites, which can reset each other's generator potentials. A single GTO afferent response is nonlinearly related to the tension produced by the inserting

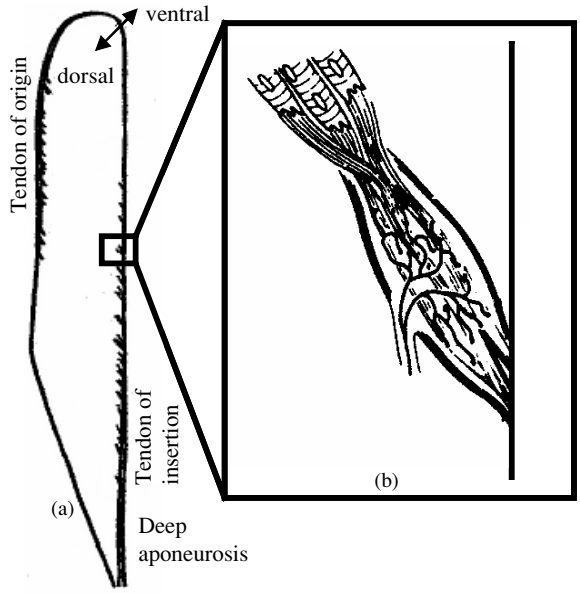

Figure 1. The distribution and structure of the biological Golgi tendon organs. (a) The cat's right medial gastrocneimus muscle with the Golgi tendon organs occupying the area of muscletendon junctions at both ends of the muscle fascicles. (b) Enlarged sketch of single Golgi tendon organ in series between the muscle fibers and tendon. Modified from Proske (1981) and Reinking *et al* (1975).

muscle fibers and the order and timing of their respective activation.

The sensory output from an individual GTO reflects the tension of the limited number of MUs that insert their fibers into its capsule, but it is an unreliable indicator of total muscle tension that results from the tensions of all MUs in the muscle. The ensemble firing of all GTO receptors in the muscle has been hypothesized to correlate better and represent a more reliable measure of the whole muscle force (Crago *et al* 1982, Houk and Henneman 1967, Reinking *et al* 1975). In experiments by Jami (Gandevia 1996, Jami 1992), simultaneous afferent recordings were obtained from ten GTOs in the peroneus tertius muscle of a cat during electrical stimulation of several MUs. Stimulation of two MUs produced almost double the muscle tension of one MU, but the total afferent activity from all GTOs was approximately equal to the sum of the activity in each GTO when acted upon by only the MU having the largest effect on that GTO. On the other hand, the ensemble firing of all the GTOs in the muscle during activation of multiple MUs was found to increase linearly with the increase in force. These observations suggest that the ensemble of GTOs could be used to compute muscle force accurately from the sum of all GTO afferent activity in the muscle. While experimental data suggest that small ensembles of GTOs can provide information about whole muscle force, there is still disagreement about the fidelity of this information (Jami 1992), particularly under the full range of physiological and artificial (e.g. prosthetic) recruitment.

This study was designed to explore the reliability of the ensemble sensory information, i.e. to study the relationship between the aggregate GTO activity and total muscle force. In order to do so, several models were constructed and combined: a statistical model of distributions of muscle fibers and GTOs in the cat's medial gastrocnemius (MG) muscle, a model of muscle force output under various conditions of recruitment (Cheng *et al* 2000) and a new model of transduction in individual GTOs (Mileusnic and Loeb 2006). The relationship between the aggregate GTO activity and whole muscle tension was investigated under natural conditions of muscle recruitment and natural distribution of GTOs and MU muscle fibers as well as in pathological muscles. Our model of GTO activity in reinnervated muscles does not take into account any reorganization of the afferent neurons that innervate them or their central projections, however. Several studies suggest that following surgical repair of severed muscle nerves, only a portion of the receptors are reinnervated (30–75%; Banks *et al* 1985, Scott 1991, 1996) and that reinnervation may be by an inappropriate afferent modality (i.e. spindle afferents can innervate GTOs). Furthermore, a more recent study suggests that while a substantial number of afferents re-establish connections with the appropriate receptors, there appears to be a central suppression of information encoded by these afferents (Haftel *et al* 2005). In addition to studying ensemble GTO activity in natural and reinnervated muscles, we also studied cases of artificial recruitment by functional electrical stimulation (FES) applied to muscles or their nerves, and frequency-modulated reversed recruitment of MUs such as that observed during cutaneous reflexes (Buller *et al* 1978, Datta and Stephens 1981). Force generation via these alternative recruitment schemes is of interest to rehabilitation therapists and neuroprosthetists and has not been studied systematically, so we have included detailed plots of the contributions of the various MUs to total active muscle force.

2. Methods

The cat's MG muscle was chosen to study the relationship between the aggregate GTO activity and whole muscle tension for two reasons. First, the MG is a fairly typical heterogeneous muscle in which three types of muscle fiber types (slow (S), fast-twitch non-fatigable (FR) and fast-twitch fatigable (FF)) are unevenly distributed across the muscle, making it possible to study how different distributions affect the ensemble GTO properties. Second, there is an extensive literature describing the distribution of muscle fibers, MUs and GTO receptors within this muscle.

Three separate models were constructed in the MATLAB modeling environment, and then combined. The recently developed GTO model (Mileusnic and Loeb 2006) was employed in order to obtain the afferent activity of each individual GTO in response to tensions of muscle fibers inserting into its capsule. Next, a model of the cross-sectional area of the MG's muscle–tendon junction (including the distributions of various types of muscle fibers, MUs and GTOs) was designed in order to obtain a realistic sample of muscle fibers that insert into each GTO receptor. Finally, the tensions of the fibers inserting into individual GTOs were calculated by using the realistic muscle model. In the following sections, the three models will be discussed in more detail.

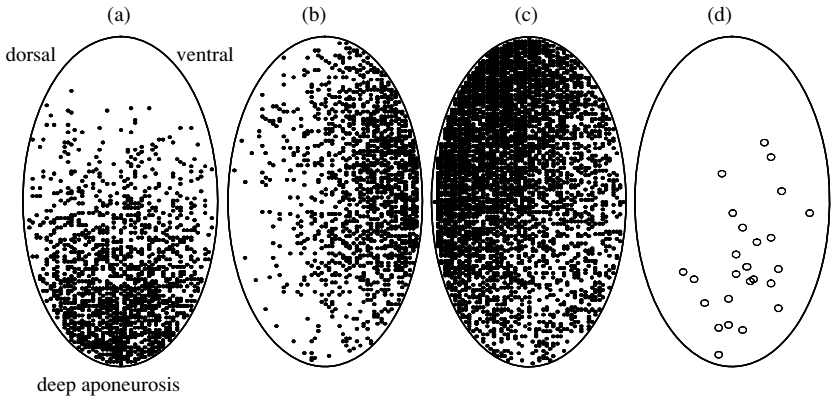

Figure 2. The modeled cross-sectional area of the muscle–tendon junction (aponeurosis of insertion) of the cat's right medial gastrocnemius. The three types of muscle fibers are distributed nonuniformly across the junction (S fibers: a; FR fibers: b; FF fibers: c). The Golgi tendon organs are also unevenly distributed across the junction (d) favoring the area of the muscle that is also densely inhabited by the S muscle fibers.

2.1. The GTO model

The recently available GTO model (Mileusnic and Loeb 2006) is a physiologically realistic mathematical model whose elements correspond to anatomical features of the biological receptor. The mechanical interactions of these elements enable the model to capture all salient aspects of GTO afferent behavior reported in the literature. The model assumes the existence of two collagenous structures in the receptor capsule: the bypassing and the innervated collagen. The afferent endings are located only in the central, innervated collagen and arise from two major branches of the Ib axon (proximal and distal), each having its own impulse-generating site. The GTO afferent output results from the competition between the afferent outputs from these two transduction zones. In order to distribute the fiber's collagen between the bypassing and innervated collagen zones, the conceptual flower-shaped model of GTO cross-sectional area was designed for every GTO in the muscle to account for their different muscle fiber compositions. For the purpose of our modeling, we assumed that the fiber's innervated collagen was evenly distributed between the two transduction zones.

2.2. The cross-sectional model of the muscle–tendon junction

In order to create realistic populations of GTOs, we modeled the distribution of muscle fibers, MUs and GTOs across the cross-sectional area of the muscle–tendon junction (the aponeurosis of insertion; see figure 2) of the cat's MG muscle. The first part of this section will deal with the intact (natural) muscle where fibers belonging to one MU are spread widely across the muscle. The second part will deal with the reinnervated muscle where MU mosaic in the muscle is significantly altered.

2.2.1. Natural muscle. The cross-sectional area of cat's MG muscle–tendon junction is somewhat elliptical in shape and was assumed to be perfectly elliptical in our model (see figure 2) (Burke 1981, Reinking *et al* 1975). An estimated 141 180 heterogeneously distributed muscle fibers can be found occupying this area with the majority of them inserting directly into the tendon and only a small portion inserting into the GTO receptors (see appendix A and table 1 for details on the numerical estimates used). With the goal of reducing the computational burden, we downsized the total number of fibers in our model by a factor of 25 (resulting in 5654 fibers distributed among 1/5 of the normal number of MUs each with 1/5 of the normal innervation ratio; see below). In order to design the cross-sectional area, a matrix of size 135 by 55 was created. Matrix fields that were enclosed by the ellipse (long and short axis equal to 135 and 55, respectively) were selected as belonging to the cross-sectional area of the muscle (given value 1) while the other fields were designated as not being part of it (given value 0). The particular dimensions for the cross-sectional area represent approximately the downsized version of the realistic MG's cross-sectional area (Reinking *et al* 1975).

Once the ellipse was created, it was necessary to assign the fibers to the specific fiber types (S, FR or FF). The literature suggests that on average 23% type S, 21% type FR and 56% type FF (see table 1) fibers can be found in the MG, and that they are non-uniformly distributed throughout the muscle (Burke and Tsairis 1973). The slow twitch fibers most densely occupy deep sections of the muscle, which distally represents the area of deep aponeurosis that leads to the tendon of insertion (see figure 2(a)). The FR muscle fibers favor the ventral areas of MG's cross-sectional area with their density decreasing toward the dorsal area (figure 2(b)), while the FF fibers favor the opposite distribution (having the largest density across the dorsal area and decreasing their density toward the deep and ventral portions; figure 2(c)). The modeled muscle fibers were distributed according to these literature observations, as indicated by the dots.

Next, the muscle fibers had to be organized into MUs. In the biological MG, some 70 S, 68 FR and 132 FF MUs (table 1) can be found; these numbers were downsized in our model by a factor of 5 (14 S, 14 FR and 26 FF) (table 2). The average sizes of MUs (innervation ratio or fibers/MU) differ for different muscle fiber types found in the cat's MG (S: 462, FR: 439, FF: 598; see appendix B, table 1). For the purpose of

Table 1. Medial gastrocnemius muscle fiber and motor unit data.

	Burke and Tsairis (1973)	Burke (1981)	Foehring *et al* (1986)	Mean values
Fiber composition (%)				
S ($percent_S$)	24.5	24.5	21	23
FR ($percent_{FR}$)	20.2	20.2	23	21
FF ($percent_{FF}$)	55.3	55.3	56	56
Whole muscle cross-sectional area PCSA (cm^2) (Spector *et al* 1980)				4.96
Individual fiber cross-sectional area (μm^2)				
S (CSA_S)	1734	1980	1970	1895
FR (CSA_{FR})	2890	2370	2264	2508
FF (CSA_{FF})	5290	4503	3873	4555
Calculated total number of fibers (see the text)				141 180
Total number of MUs (average from Burke *et al* (1977), Boyd and Davey (1966, 1968))				270
MU composition (%) (in parentheses is the actual number of MUs)				
S	28	25.2	24	26 (70)
FR	28	23	24	25 (68)
FF	44	51.9	52	49 (132)
Indirect innervation ratio (fibers/MU)				
S				462
FR				439
FF				598

Table 2. Medial gastrocnemius muscle fiber and motor unit composition parameters that were employed in designing the Virtual Muscle model.

	S	FR	FF
Number of motor unit of particular fiber type	14	14	26
Fraction of MG's PCSA that is occupied by particular fiber type	0.125	0.156	0.719

our modeling, the average innervation ratios were downsized by a factor of 5 (S: 92, FR: 88, FF: 120). The MUs within a given fiber type also exhibit a range of sizes. The Virtual Muscle program includes an algorithm that apportions the total cross-sectional area of the muscle fibers of each specific type into MUs that reflect their different innervation ratios (Cheng *et al* 2000). Once each MU's innervation ratio was determined, its muscle fibers were distributed randomly among a pool occupying one-third of the total cross-sectional area of the muscle–tendon junction (Burke and Tsairis 1973).

Finally, the GTO receptors had to be distributed across the muscle–tendon junction. Typically, some 44 GTO receptors can be found occupying the cat's MG, where 25 are located along the aponeurosis of insertion and 19 along the aponeurosis of origin (Swett and Eldred 1960). Similar to the muscle fiber types, the GTOs are also unevenly spread across the aponeurosis of insertion, with a higher concentration in the deep areas of the muscle that are more densely populated by the S muscle fibers (Reinking *et al* 1975, Swett and Eldred 1960). Twenty-five distal GTOs were distributed in our model according to these observations (figure 2(d)). The effect of ignoring the 19 GTOs at the origin would be a modest reduction in the total amount and an increase in the noisiness of the ensemble activity. The effects of downsizing the modeled population of MUs would be expected to be a modest increase in the granularity of muscle force, which may have accentuated the nonmonotonic relationships observed between GTO activity and muscle force, particularly in models of electrical stimulated muscle (see below).

Once the location of individual GTOs within the cross-sectional area was determined, the muscle fibers lying in the vicinity of the receptor were selected as the ones inserting into the GTO capsule. The experimental data suggest that on average, some 20 muscle fibers belonging to 13 different MUs insert into each MG GTO (Gregory 1990). Because in a biological GTO a MU typically contributes either 1 or 2 of its fibers to the receptor, in our model 13 fibers located closest to each GTO receptor and belonging to different MUs were selected. Out of these 13 MUs, 7 of them were randomly selected as the ones contributing the second muscle fiber to the receptor, bringing the total number of fibers inserting into the receptor to 20.

2.2.2. Reinnervated muscle. In the intact MG muscle, a single MU is composed of fibers of the same muscle fiber type that are distributed sparsely throughout a relatively wide area of the muscle (motor territory; Burke and Tsairis 1973). In a muscle with mixed fiber types, adjacent muscle fibers are likely to be of different fiber types, as well, producing a fine 'mosaic' pattern in histological studies of single MUs or fiber type distributions. Following a peripheral muscle nerve injury, crushed or severed motor axons degenerate distally but start to regrow outward from the proximal, intact portion of the nerve. Most muscle fibers are eventually reinnervated, but often not by the motor axons that originally serviced them (particularly if the nerve was cut, whether surgically repaired or not). The reinnervating motor axons tend to innervate the first available

muscle fibers they encounter in the muscle, giving rise to MUs that are composed of different types of muscle fibers that are densely packed into relatively small motor territories. During this period, the relationship between the contractile speed and tension of MUs differs from that measured in the original muscle prior to injury (Lewis 1972, Warszawski *et al* 1975). Over a period of several months following the reinnervation, the reinnervated MUs become homogeneous again (Kugelberg *et al* 1970), suggesting that the motor nerves respecify the histochemical properties of the muscle fibers they supply, most likely as a result of the trophic effects of their different patterns of recruitment (Jarvis *et al* 1996). Relatively normal relationships between the MU's contractile speed and tension are typically re-established (Gordon and Stein 1982), but the mosaic of interdigitated MUs remains severely disturbed. The relative sizes of MUs and types are also re-established and are representative of the ones observed in the normal muscle; however, the recruitment order of the MUs in the muscle might vary. A muscle that is reinnervated by the same motor axons that initially innervated the muscle (self-reinnervated muscle) re-establishes the MU recruitment pattern observed in the natural muscle (Cope and Clark 1993, Gordon and Stein 1982). However, reinnervation by motor neurons that originate from a different motor pool than that before the injury demonstrate highly abnormal recruitment patterns (Gordon 1988, Gordon and Stein 1982).

In order to study the relationship between the aggregate GTO activity and whole muscle force, it was necessary to introduce some changes to our model. In designing the cross-sectional model of the muscle–tendon junction of reinnervated muscle, the same shape and percentage fiber composition were employed as for the natural muscle. The muscle fibers belonging to a single MU were packed into a very small area within the muscle, however, and not located across 1/3 of cross-sectional areas as in the case of natural muscle. Furthermore, while the distribution of GTOs was unaltered, the limitation that a single MU contributes only one or two muscle fibers to a single GTO was removed. Therefore, GTOs in the reinnervated muscle tended to have several muscle fibers belonging to the same MU inserting into them.

2.3. Realistic muscle model

A realistic MG muscle model was designed by employing the Virtual Muscle model (Cheng *et al* 2000). Virtual Muscle is a sophisticated Hill-type muscle model that allows the user to specify the particular muscle's morphometric data, muscle fiber and MU composition and the MU recruitment properties in order to calculate the tension the muscle generates in response to specific patterns of excitation applied to the motor pool.

For the purpose of designing a realistic MG model, certain morphometric data about the MG had to be collected from the literature. Because it was not possible to obtain the entire set of morphometric data from a single cat preparation, we made an effort to use the preparations in which cat weights were comparable. Values of some of the parameters, such as muscle mass, optimal fascicle length or maximal whole muscle length, were readily available while the length of the tendon at the muscle's optimal force had to be calculated indirectly (see appendix C). For the purpose of running the Virtual Muscle model, the muscle–tendon path was set to be at the constant length (11.66 cm) that placed inactive fascicles at their optimal length. The percentage of the total muscle cross-sectional area that was occupied by a single muscle fiber type was obtained by multiplying the total number of muscle fibers of a particular type in the muscle with the individual fiber's cross-sectional area and dividing it by the whole muscle cross-sectional area. Finally, we assumed the muscle's cross-sectional area to be equal to 1/25 of the experimentally measured value, given that both the number of MUs and innervation ratio were reduced by a factor of 5. Because Virtual Muscle calculates the cross-sectional area internally from muscle mass and fascicle length values, the mass necessary to obtain the desired cross-sectional area was equal to 0.503 g. When scaled by a factor of 25 (12.5 g), the muscle mass used in our model is representative of a large size cat; somewhat lower values of MG mass were reported in the medium size cat (9.8 g; Spector *et al* 1980). The morphometric data used in designing the Virtual Muscle model are listed in table 3 while the muscle fiber and MU composition are provided in table 2. Finally, it should be mentioned that the available experimental data suggest that the largest S MUs have a larger cross-sectional area than the smallest four FF MUs' cross-sectional area. This is contrary to the common assumption that all the S MUs are smaller than the FR MUs, which are in turn smaller than FF MUs (Henneman's size principle; Henneman and Olson 1965, Henneman *et al* 1965). Our model had a distribution of unit sizes and types that reflected the actual data. The details of their recruitment under various simulated conditions are provided below. Once all the muscle-specific data were collected, a MATLAB Simulink block of the cat's MG was created. While the model typically provides only whole muscle tension, certain modifications were introduced to the Simulink block in order to extract the tensions of individual MUs in the muscle. The individual fiber tension was calculated by dividing the MU tension by the MU innervation ratio.

Table 3. Medial gastrocnemius morphometric data that were used in designing the Virtual Muscle model.

Parameter	Parameter value	Reference
Muscle mass (g)	0.503	See section 2
Optimal fascicle length (cm) (L_0^f)	2.4	Griffiths (1991)
Tendon length at the muscle's optimal force (cm) (L_0^T)	9.9	See appendix C
Whole muscle maximal passive length (cm) ($L^{WM}_{max\_passive}$)	12.5	Goslow (1973)

2.3.1. Virtual Muscle recruitment patterns. Four different types of MU recruitment were analyzed in this study: natural frequency-modulated MU recruitment, reversed frequency-modulated MU recruitment, and electrical recruitment by intramuscular (IM) and nerve cuff (NC) electrodes. Two

excitation profiles were applied to each of these four recruitment profiles. A very slow ramp (81 s duration) in which both contractile and transduction dynamics were negligible was used to understand the relationship between GTO activity and steady-state force over the full range of recruitment (Virtual Muscle ignores long-term physiological effects such as fatigue and assumes that fast twitch muscle fibers are operating in the fully potentiated state; Brown and Loeb 1998). A phasic excitation pattern was designed to approximate the sensory and motor activity that might occur during a cyclical behavior such as locomotion; parameters are included in section 3.

Natural frequency-modulated MU recruitment. Virtual Muscle was designed primarily to model the behavior of muscles during the natural recruitment of MUs. During natural recruitment, all the S MUs are recruited prior to the recruitment of the first FR MU, and the FF MUs are the last to be recruited in the muscle. The recruitment of the MUs of the same muscle fiber type also follows the size principle rule where the smaller MUs are recruited prior to the larger ones. Finally, individual MU activity is frequency modulated over a range of firing rates that depends on the fiber type, as is observed naturally. Virtual Muscle normalizes firing rates to $f_{0.5}$, the frequency at which a given fiber type reaches half of its maximal tetanic force at an optimal, isometric length. The range of firing rates for all fibers was 0.5–2.0 times $f_{0.5}$.

Reversed frequency-modulated MU recruitment. In addition to using Virtual Muscle to study natural recruitment, the model was also employed to study the muscle tension during reversed frequency-modulated MU recruitment. During the late 1970s and early 1980s, several studies applied cutaneous stimulation during voluntary contraction of human first dorsal interosseous muscle in order to demonstrate MU recruitment order contrary to Henneman's size principle (Buller *et al* 1978, Datta and Stephens 1981). While the exact recruitment order of all MUs in the muscle during these experiments was never explicitly obtained, it was demonstrated that cutaneous stimulation shifts the weighting of synaptic input associated with a voluntary contraction to favor the activity of the more powerful fast twitch MUs. Recruitment order in the decerebrate cat appears to be less susceptible to alteration (Clark *et al* 1993, Prather *et al* 2002) but motoneuron activity patterns during decerebrate locomotion are known to be different than those in intact cats (Hoffer *et al* 1981). In fact, individual motoneurons exhibit rather complex modulations in their firing during cutaneous reflexes in the intact, walking cat (Loeb *et al* 1987), so we elected to model the extreme case where the MUs are frequency modulated but their recruitment order is completely reversed. In other words, the first MU being recruited was the largest FF and the last recruited was the smallest S MU.

Electrical recruitment by IM and NC electrodes. Finally, Virtual Muscle was employed to model muscle tension during the reanimation of paralyzed limbs by means of electrical stimulation (IM and NC electrodes). In patients where paralysis results from lesions of upper motor pathways (e.g. stroke and spinal cord injury), the motoneurons, peripheral nerves and muscles are typically spared, making it feasible to stimulate the large myelinated axons of the motoneurons in order to produce muscle contraction. Depending on where the motoneuron stimulation is applied (e.g. intramuscular, peripheral nerve, motor nuclei), at least some proprioceptive afferents including those innervating the GTOs are likely to be recruited as well. The IM electrode is most commonly placed near the nerve entry zone, where the muscle nerve divides into progressively finer branches on its way to innervate individual compartments and fascicles in the muscle. The larger motor axons (innervating FR and FF MUs) are generally more excitable than smaller motor axons (innervating S MUs), but the actual recruitment produced by IM stimulation tends to be more random than size-related for two reasons (Singh *et al* 2000). The first is that recruitment tends to be dominated by the relative distance of the motor axon from the IM electrodes, which varies greatly depending on which intramuscular nerve branches carry its axons. The second is that the larger motor axons tend to have higher innervation ratios and larger motor territories. Each time they bifurcate, motor axons become smaller in caliber, so the intramuscular branches of all motor axons are more homogeneous than they are in the main muscle nerve. Several profiles of muscle tension during the IM FES exist in the literature (Cameron *et al* 1998) and demonstrate somewhat step-like behavior consistent with this recruitment scheme. A gradual increase in stimulation strength produces a muscle tension profile with several discrete steps (i.e. recruitment of axons in a new nerve branch) and more gradual increases within those steps (i.e. progressive recruitment of axons within a given nerve branch). The detailed description of the MU recruitment algorithm that we implemented into Virtual Muscle in order to obtain the MU tensions during the IM electrode stimulation is presented in appendix D.

An alternative to the IM electrode is the NC electrode which wraps around a muscle nerve. The NC electrode produces relatively homogeneous field strength in all parts of the nerve, depolarizing the axons in proportion to their size. The larger axons innervating larger fatigable MUs tend to be activated first and the smaller axons innervating smaller fatigue-resistant MUs last (Solomonow 1984). Therefore, the NC stimulation results in a recruitment pattern that is opposite to that during physiological recruitment (Blair and Erlanger 1933, Fang and Mortimer 1991). Additionally, the size principle among the MUs of the same fiber type tends generally to be also reversed from physiological recruitment, with the largest MUs of the particular muscle fiber type recruited prior to the smaller MUs of the same muscle fiber type. This is similar to the reversed recruitment order modeled for cutaneous reflexes but without the frequency modulation. The described recruitment modifications were implemented in the Virtual Muscle model for the purpose of our modeling study and the new MG model was created and run in MATLAB Simulink.

3. Results

The results are divided into five sections. First, the aggregate GTO activity is presented during gradual physiological

recruitment of normal muscle where muscle fibers belonging to numerous MUs and GTOs are naturally distributed and the MUs are naturally recruited. In the next two sections, a similar analysis of ensemble GTO activity is performed but during gradual physiological recruitment of reinnervated muscle and during frequency-modulated reversed recruitment of MUs. The fourth section deals with the gradual electrical stimulation of normal muscle by two electrodes (IM and NC) that produce different recruitment orders. Finally, the GTO-ensemble activities are compared during phasic excitation of the healthy and reinnervated muscle and during IM and NC electrode stimulation.

3.1. Ensemble GTO activity during gradual physiological recruitment of a normal muscle

The tensions of fibers inserting into each GTO were obtained by specifying the natural recruitment option in Virtual Muscle as described in section 2. The model was supplied with ramp excitation that started at 0 (no recruitment) at time 1 s and reached 1 (the maximal muscle excitation) at time 81 s. The fractional excitation level at which all MUs are recruited (Ur; i.e. the threshold for the last MU recruitment) was set to 0.8 in Virtual Muscle as suggested by Cheng *et al* (2000). Between the excitation level of 0.8 and 1, all the MUs were only frequency modulated; all of them reached their maximal firing rate when excitation reached 1. The dynamic terms of muscle activation and GTO transduction are all much faster than this ramp, so this unphysiologically long contraction serves to illustrate the effects of each successive MU recruitment without distorting static muscle force.

Once the individual GTO fiber compositions were identified and tensions of individual fibers were obtained, 25 GTO models were created and their outputs summed to provide the ensemble GTO activity (figures 3(a) and (c)). During the first 10 s, the ensemble activity rises relatively rapidly as a result of activation of S MUs that produce little tension but strongly excite the GTOs. The later recruitment of FR and FF MUs results in a faster increase in tension but a much slower rise in the ensemble GTO activity. The ensemble GTO activity was plotted against the whole muscle tension in order to study the ability of the aggregate activity to monitor the whole muscle tension (figure 7(a)). The results are nonlinear but monotonic, with an initially steep slope from recruitment and frequency modulation of S MUs, followed by a flatter slope as muscle fibers from type FR and FF MUs generate more tension but less incremental activity in GTO afferents.

3.2. Ensemble GTO activity during gradual physiological recruitment of a reinnervated muscle

The cross-sectional model of muscle fiber, MU and GTO distributions of reinnervated muscle that is described in section 2 was used. The size-ordered recruitment of MUs during the slow ramp was the same as for section 3.1 (physiological recruitment of a normal muscle). The individual MU tensions, whole muscle tension and GTO ensemble activity are shown (figures 3(b) and (c)), as well

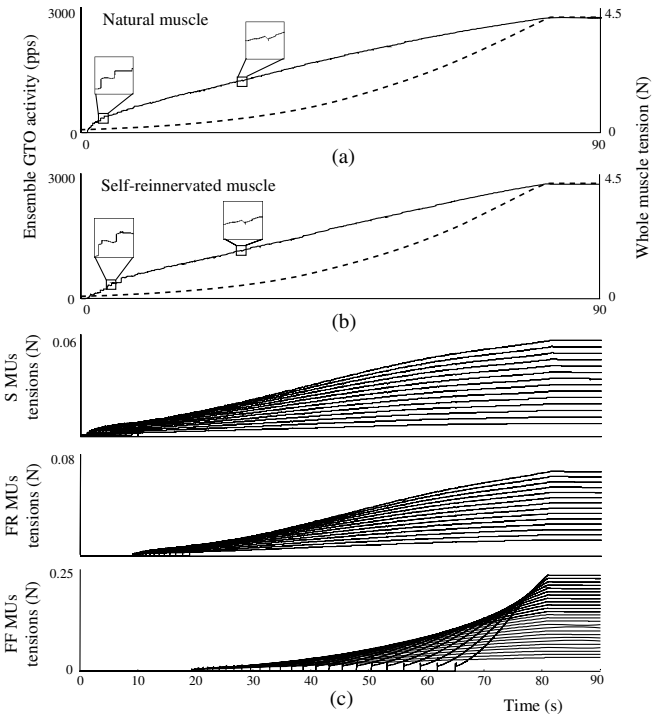

Figure 3. The ensemble Golgi tendon organ activity during gradual physiological recruitment of healthy and self-reinnervated muscle. (a) The total muscle tension during gradual physiological recruitment of healthy muscle (lower curve, right scale) and the cumulative activity of 25 Golgi tendon organs (upper curve, left scale). (b) The total muscle tension during gradual physiological recruitment of reinnervated muscle (lower curve, right scale) and the cumulative activity of 25 Golgi tendon organs (upper curve, left scale). (c) The tensions of individual MUs in the muscle.

as the relationship between the ensemble GTO activity and whole muscle tension (figure 7(b)). Surprisingly, our model suggests that the distortion of the MU territories following the reinnervation does not substantially affect the relationship between the aggregate GTO activity and muscle tension. It is only slightly noisier than in the normal muscle at low recruitment levels (compare insets in figures 3(a) and (b)), presumably because each GTO now responds to the tension in only a small number of densely packed MUs rather than sampling from 10 to 20 different, highly intermingled MUs.

3.3. Ensemble GTO activity during reversed frequency-modulated recruitment

As described in section 2, we modified Virtual Muscle so that individual MUs were frequency modulated, but the first MU recruited was the largest FF and the last recruited was the smallest S MU. The model was supplied with ramp excitation that started at 0 at time 1 s and reached 1 at time 81 s. The fractional excitation level at which all MUs are recruited was set to 0.8. The ensemble GTO activity (figure 4) deviates significantly from the ones observed during the recruitment of healthy and reinnervated muscle by having the opposite concavity. This is reflected in the more linear relationship between the ensemble GTO activity and muscle force (figure 7(c)).

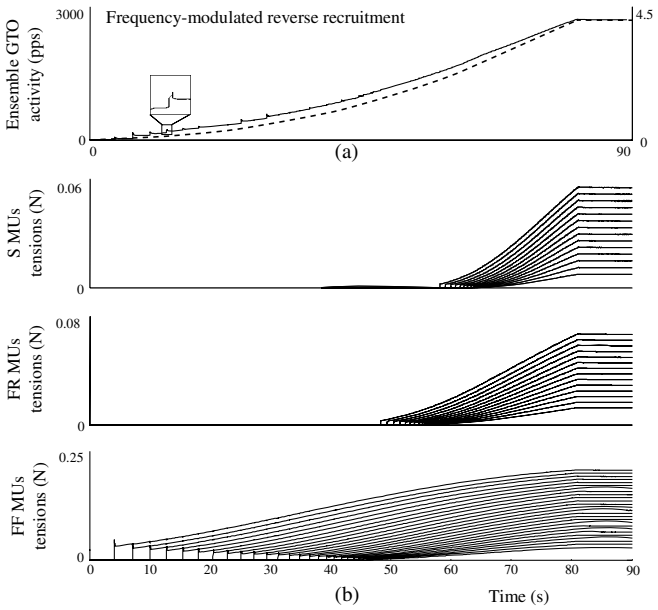

Figure 4. The ensemble Golgi tendon organ activity during the frequency-modulated reversed recruitment of MUs. (a) The total muscle tension (lower curve, right scale) and the cumulative activity of 25 Golgi tendon organs (upper curve, left scale). (b) The tensions of individual motor units in the muscle.

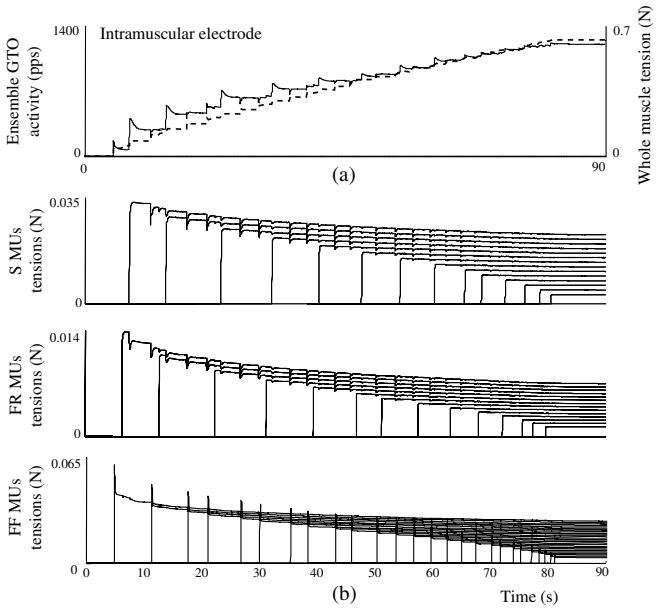

Figure 5. The ensemble Golgi tendon organ activity during the intramuscular electrode stimulation. (a) The total muscle tension (lower curve, right scale) and the cumulative activity of 25 Golgi tendon organs (upper curve, left scale). (b) The tensions of individual motor units in the muscle.

3.4. Ensemble GTO activity during gradual electrical stimulation of muscle

3.4.1. IM electrode stimulation. IM electrical stimulation was modeled as random for the various MUs and fiber types (see section 2 and appendix D). The stimulation pulse intensity was increased in a slow ramp from zero to maximal recruitment (0–1 in 81 s) while the pulse frequency was kept constant at 20 pps. The fractional excitation level at which all the MUs are recruited in the muscle (Ur) was set to 1 because once the MU is recruited there is no frequency modulation of its firing rate. The GTO ensemble activity versus time curve (figure 5) and the relationship between the GTO aggregate activity and muscle tension (figure 7(d)) demonstrate very irregular characteristics. Note also that both the maximal muscle tension and the maximal ensemble GTO activity are substantially reduced because the fixed 20 pps firing rate is substantially lower than that would be achieved by maximal physiological recruitment.

3.4.2. NC electrode stimulation. NC electrical stimulation was modeled as reverse recruitment order from the size principle (see section 2). Gradually ramped stimulation intensity (0–1 in 80 s) was supplied to the model while the pulse frequency was kept constant at 20 pps, similar to 3.4.1 IM stimulation. The GTO aggregate activity (figure 6) as well as the relationship between the ensemble GTO activity and whole muscle tension during the NC stimulation (figure 7(e)) is significantly distorted from the relationships in healthy muscle.

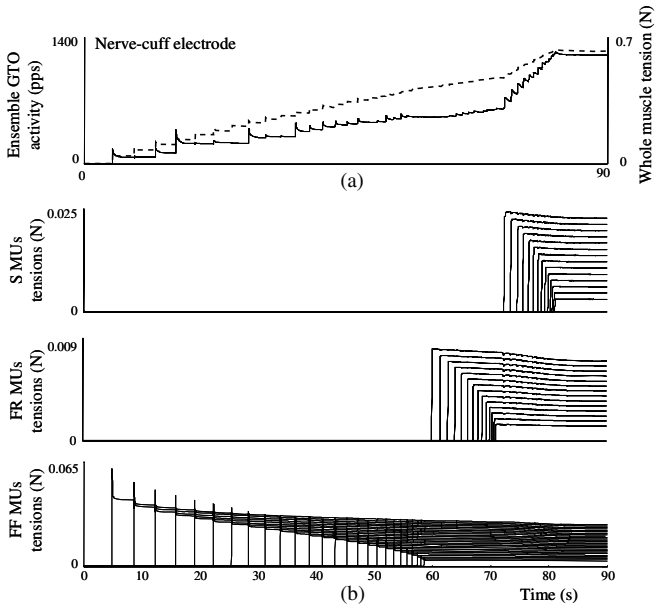

Figure 6. The ensemble Golgi tendon organ activity during the nerve-cuff electrode stimulation. (a) The total muscle tension (upper curve, right scale) and the cumulative activity of 25 Golgi tendon organs (lower curve, left scale). (b) The tensions of individual motor units in the muscle.

3.5. Ensemble activity during phasic excitation

The ramp activation times that we employed in our first analysis were very long in order to study the details of the ensemble GTO activity under quasi-static conditions. During natural tasks, however, activation times are usually on the order of hundreds of milliseconds. In order to study the ensemble GTO characteristics under such conditions, we designed a

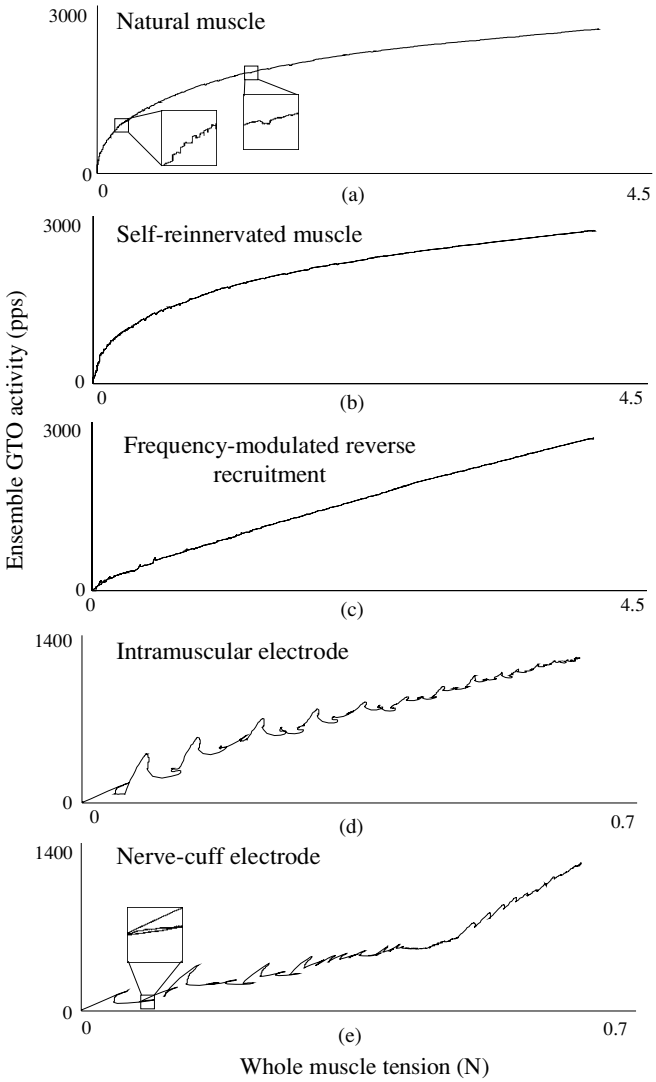

Figure 7. The relationship between the ensemble Golgi tendon organ activity and whole muscle tension. The relationship is shown for five conditions studied: the intact muscle (a); self-reinnervated muscle (b); frequency-modulated reversed recruitment (c); intramuscular electrode stimulation (d) and nerve-cuff electrode stimulation (e). Note that the maximal aggregate Golgi tendon organ activity during intramuscular and nerve-cuff electrode stimulation is about half of the activity observed in healthy and reinnervated muscle; the corresponding tension levels are even lower.

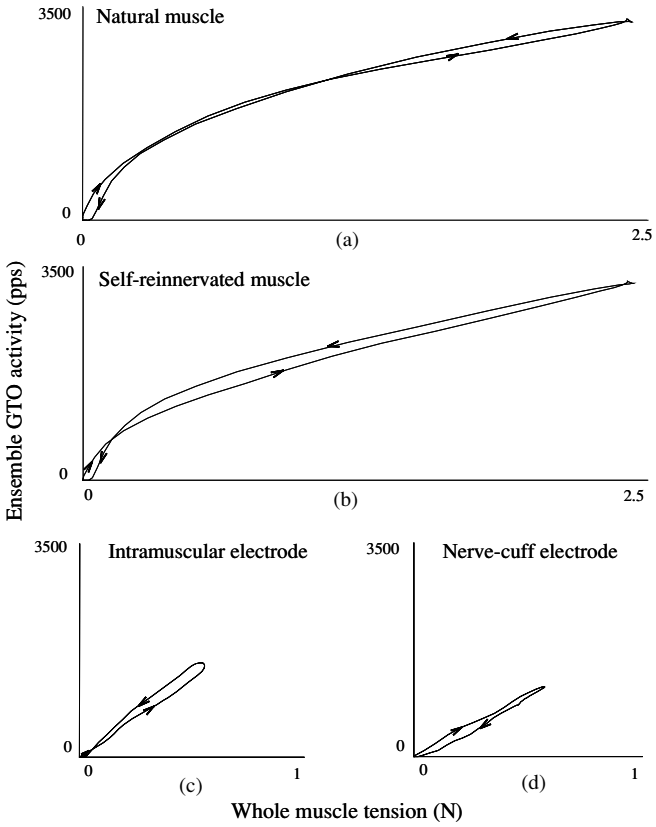

Figure 8. The relationship between the ensemble Golgi tendon organ activity and whole muscle tension during the phasic muscle excitation. The aggregate activity was studied during the activation pattern that consisted of a ramp excitation rise (from 0 to 0.8 in 150 ms), sustained excitation at 0.8 (for 200 ms) and a ramp excitation fall (from 0.8 to 0 in 150 ms). The relationship is shown for four conditions: intact muscle (a); self-reinnervated muscle (b); intramuscular electrode stimulation (c) and nerve-cuff electrode stimulation (d).

muscle excitation pattern more representative of those found during repetitive natural movements such as locomotion. It consisted of a rapid excitation ramp up (0–0.8 in 150 ms), a hold at 0.8 for 200 ms and a ramp down (0.8–0 in 150 ms). The fractional activation level at which all the MUs are recruited in the muscle (Ur) was set to 1 for the IM and NC electrode stimulation cases and to 0.8 for the case of the intact and reinnervated muscle. During natural recruitment of both normal and reinnervated muscle, the relationship between the GTO aggregate activity and muscle force was nonlinear but closely matched during the rise and fall of excitation (figures 8(a) and (b)). For both types of FES stimulation, the relationships were more linear and closely matched during the rise and fall of excitation (figures 8(c) and (d)). Note that the maximal aggregate GTO activity during IM and NC electrode stimulation is about half of that observed in healthy and reinnervated muscle while maximal muscle tension is about 25%.

4. Discussion

Once considered as the protective organ that discharges only at high muscle tensions, the GTO's role was reevaluated when it was demonstrated to be capable of accurately monitoring active muscle tension over a much wider range than initially thought (Alneas 1967, Crago *et al* 1982, Houk and Henneman 1967). The aim of this study was to consider the fidelity of aggregate GTO information because individual GTO activity has been shown to be a poor indicator of whole muscle force. Our analysis shows that aggregate GTO activity could be utilized by the central nervous system (CNS) to obtain accurate muscle tension information during physiological recruitment of normal and reinnervated muscle according to the size principle. In contrast, electrical stimulation or physiological reversal of the MU recruitment (e.g. due to cutaneous reflex

effects) significantly alters the natural relationships between muscle tension and aggregate GTO activity.

The relationship between the aggregate activity and whole muscle force in a normal muscle during natural recruitment has the shape of a saturating exponential curve (figures 3(a) and 7(a)). Several factors contribute to the particular shape. The distribution of MU types and GTOs in a typical mixed muscle such as MG tends to over-represent type S muscle fibers in the population inserting into the ensemble of GTOs. The percentage of myotendinous collagen that enters the loosely packed, transduction zone of the GTO is higher for the smaller type S fibers than for the larger type FR and FF fibers. Most importantly, however, the GTO generates a disproportionate amount of afferent activity in response to whatever muscle fibers are active first, which are the type S fibers in normal muscles recruited physiologically. The natural recruitment of S and FR MUs in the normal muscle results in dynamic peaks in both the curve of the ensemble GTO activity versus time and the aggregate GTO activity versus muscle tension (see insets on the first portions of the curves in figures 3 and 7). Surprisingly, the recruitment of FF MUs results in small valleys instead of peaks in both curves as a result of the tension profile of the FF MUs. While the recruitment of S and FR MUs results in a smooth tension increase, the tension profile of the FF MU recruitment consists of a brief dynamic peak that decays (i.e. 'sags') within approximately 100 ms following the recruitment (see figure 3). The observed dynamic peak results in a small, brief stretch of the tendon and relieves the active S and FR fibers that insert into GTOs of some of the tension. The net effect of the increase in FF MU's tension and the decrease in the active S and FR MUs' tensions is a brief decrease in the ensemble GTO afferent firing because of the over-representation of S fibers in the GTO population.

The aggregate GTO activity in reinnervated muscle (figures 3(b) and 7(b)) was well correlated with total muscle tension despite the disruption of the normal mosaic of MU territories and its profound impact on the sampling of MUs and fiber types by each GTO. While a single S MU typically contributes one or two of its fibers to several GTOs in the intact muscle, in the reinnervated muscle a single S MU contributes many fibers to one or two GTOs. Because the potency of a single MU that has few fibers inserting into several GTOs is the same as if it had more fibers inserting into fewer GTOs (due to the nonlinear nature of the collagen stress–strain curve), the curve of the aggregate GTO activity versus muscle force during the activation of S MUs is little distorted from that observed in the intact muscle. During the later activation of FR and FF MUs, the relationship is slightly noisier due to a few GTOs that received no input from type S fibers at all, but the net effects on the aggregate GTO activity are very small.

The ensemble GTO activity during the frequency-modulated reverse recruitment of MUs (figures 4 and 7(c)) differs significantly from that observed in the healthy or reinnervated muscle. During the recruitment of first MUs (FF), the large increase in ensemble activity is not as noticeable, but instead several large spikes are visible as the result of dynamic peaks and FF MUs' tension profile. During the later phases of the recruitment (FR and S MUs), the ensemble GTO activity is smoother and the saturation of the ensemble activity is absent as a result of the over-representation of S fibers in the GTO population. The relationship between the ensemble GTO activity and muscle force has linear characteristics. During the lower tensions, the active FF MUs excite the GTO population but at the same time produce very large tensions and therefore reduce the fast rise in the relationship during the low-tension levels observed in the healthy or reinnervated muscle. At the higher tensions, the activation of over-represented S MUs (which produce little tension but strongly excite GTOs) overcomes the saturation phenomena normally associated with the nonlinear properties of the collagen stress–strain relationship. One prediction of this model is that any perception of force based on GTO activity during such reverse recruitment would be lower than the actual force so-generated.

For both types of electrical stimulation, the relationship between the aggregate GTO activity and muscle tension differs substantially from that of naturally recruited MUs. One contributing factor is the absence of frequency modulation in recruited MUs. This is particularly significant for the S MUs because the fixed stimulation frequency (20 pps) is relatively higher on their force–frequency relationship than is that same frequency for the type FR and FF MUs. This strong, abrupt activation of a large S MU whose fibers insert into many GTOs results in large dynamic peaks in the ensemble GTO activity (figures 5 and 6). As the muscle tension builds up during the IM electrode stimulation, the dynamic peaks produced by the S MUs become smaller in size because the S MUs being activated are smaller (influencing fewer GTOs), and because of the nonlinear nature of the collagen stress–strain relationship. The activation of FF MUs results in a brisk drop in the ensemble activity for the same reasons mentioned for natural recruitment. The drop is larger than that in the case of natural recruitment, however, because the point at which the first and largest FF MU becomes active is lower on the collagen stress–strain curve than during natural recruitment and because the stimulation frequency at which each FF MU becomes active is 20 pps and remains constant rather than being gradually modulated as is the case during natural recruitment. At the same moment that the drop in the ensemble GTO activity is observed, the total muscle tension record demonstrates a brisk peak followed by the sag that is typical of FF MU activation. These two phenomena together are reflected in the relationship between the aggregate GTO activity and muscle tension during the IM electrode stimulation by the presence of 'hoops' (figure 7(d)). The activation of FR MUs also results in the presence of hoops, but of much smaller magnitude than that in the case of FF MUs because their tension profiles during the activation do not exhibit such a markedly dynamic peak.

When the NC electrode is used instead of the IM electrode to stimulate the muscle, the relationship between the aggregate GTO activity and the whole muscle force has two distinct regions (figure 6). The first part of the curve has a lower slope and results from the recruitment of FF and FR MUs in reverse size order. During the activation of FF MUs, dynamic peaks of tension followed by 'sag' are present in both the GTO ensemble record and the muscle tension record, resulting

in the very spiky curve relating the aggregate GTO activity to the muscle tension (figure 7(e)). The curve occasionally incorporates small hoops as in the case of IM electrode stimulation. During the activation of FR MUs, the dynamic peaks are not present in the tension record but only in the ensemble record and are of much smaller magnitude than that in the case of FF MUs. When the S MUs become active, the slope of the ensemble GTO activity versus muscle tension curve increases markedly. This is not only because S MUs are over-represented in the GTO population, but also because the stimulation frequency of 20 pps is much closer to the frequency necessary to tetanically stimulate S MUs than FR or FF MUs. Because the largest S MUs having many fibers in the GTOs are recruited prior to the smaller ones having fewer fibers in the GTOs, the dynamic peaks during NC electrode stimulation are initially prominent but then progressively reduce in size.

The differences in the relationship between the aggregate GTO activity and whole muscle tension for different recruitment schemes and for reinnervation are less pronounced during rapidly modulated, phasic excitation of the motor pool (figure 8). During natural muscle recruitment, the relationship between the aggregate GTO activity and tension are mostly quite similar during the excitation rise and fall. At lower tensions, the ensemble GTO activity is larger during the excitation rise than fall as a result of the dynamic peaks during individual MU activations. At larger tensions, however, the two curves cross and the opposite becomes true. While at larger tensions the dynamic peaks are still present as a consequence of the MU recruitment, the effect that they have on the GTO ensemble activity is counterbalanced by the slow activation property of S MUs. Because the tension of the S MUs rises slowly compared to the ramp upward of excitation, most of the initial muscle tension comes from fast responding FR and FF MUs. The slowly falling tension in S MUs contributes to total muscle tension and to ensemble GTO activity more significantly during the rapid deactivation phase. The presence of contracting S MUs that vigorously activate the GTOs during the early phase of falling muscle excitation results in greater ensemble GTO activity than during the late phases of increasing excitation.

In the case of reinnervated muscle and natural recruitment, the curve of the ensemble GTO activity versus whole tension looks very much like the one modeled for healthy muscle. The place where the ensemble GTO activity during the excitation rise crosses the one during the excitation fall occurs at smaller muscle tensions than that in the healthy muscle as the result of slightly greater sampling of S fibers by the GTOs in the reinnervated than in the healthy muscle. The muscle tension at which the crossing of two curves takes place is even lower for the case when the IM electrode is used to excite the muscle. This not only results from the altered recruitment order, but also from the fact that at 20 pps the S MUs are relatively more activated than FR and FF MUs. The ensemble GTO activity during the phasic excitation of the muscle by the NC electrode is always larger during the excitation rise than fall because of the absence of slowly activated S MUs (the maximal muscle excitation of 0.8 is below the recruitment threshold for any S MUs).

While the model parameters are based on experimental data, the model's sensitivity to the parameter values was not explicitly investigated. During the initial development of the models, we observed anecdotally that small variations in these parameters had little effect on the predicted whole muscle tension or GTO activity. Parameters used in designing the statistical model of the cross-sectional area of the muscle–tendon junction were all based on the experimental literature. The GTO model and Virtual Muscle model are published models that we supplied with muscle-specific data that were extracted from the experimental literature The fivefold reduction of the number of MUs in our model in comparison with natural muscle could potentially affect the smoothness of obtained ensemble GTO activities. This effect would be most noticeable in the case of uneven ensemble GTO activity as observed during electrical stimulation. The larger number of MUs present in natural muscle would result in a larger number of smaller peaks in ensemble GTO activity under conditions of electrical stimulation in comparison with activity obtained by our model. The general characteristics of this ensemble GTO activity in actual muscle should not be qualitatively different from those predicted by our model.

4.1. The role of GTO activity in the perception of force

If ensemble GTO activity is used by the CNS to monitor muscle force, it would be interesting to know how our results compare to psychophysical studies on perception. In 1953, Stanley Stevens noted that over an extended range of stimulation the intensity of a sensation is best described by a power function $I = K * (S)^n$, where K and n are constants, I is the intensity of sensation and S is the stimulus strength (Stevens 1962). This equation implies that the plot of log of intensity versus log of stimulus strength results in a straight line whose slope is the exponent n. To test how our ensemble GTO activity predictions compare to psychophysical observation, we plotted the ensemble GTO activity and whole muscle tension on log scales. The tension value of zero and extremely small tensions were excluded from the analysis because the log of zero is not defined. Therefore, we plotted the tension values after the activation of the first S MU (0.07 s following the first MU activation and before the second MU became active) to generate the log–log plot. Our analysis demonstrates an approximately linear relationship between the log of ensemble GTO activity and log of muscle force (figure 9) but the exponent (slope) is approximately 0.5 versus a reported slope of 1.7 for static muscle force perception. Stevens' exponents range from 0.3 to 1.7 for various sensory modalities, with lower values common for percepts arising from stimuli with a wide dynamic range such as brightness and loudness. It is important to note that the power law was derived for perception rather than transduction. Any constant slope on such a log–log plot confers the psychophysically salient property of ratiometric scaling, which might then be shifted by subsequent processing in the CNS.

While our findings suggest that in the healthy muscle the ensemble GTO activity could be used by the CNS to estimate accurately the muscle force, psychophysical

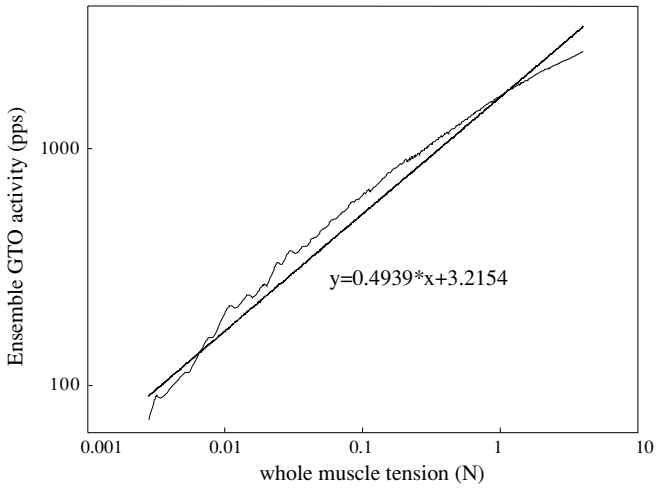

Figure 9. The log–log plot of ensemble Golgi tendon organ activity versus whole muscle force. The model prediction is compared to the best-fit straight line.

experiments suggest that sensory feedback is not the only feedback that the CNS employs in perceiving muscle force. During the 1980s, numerous force perception experiments were conducted in which the subjects estimated the force of a controlled reference contraction during changes in muscle state (for example during fatigue and tendon vibration) by generating a matching contraction of the corresponding muscle group in the other limb (Jones and Hunter 1982, 1983, 1985). The fatigue experiments were particularly interesting because the matching force in the other limb was found to be much larger than the force produced by the fatigued muscle. Therefore, the researchers concluded that efference copy from the descending command plays a major role in our perception of force, although it should be remembered that the motoneurons themselves have recurrent collaterals signaling their output to the Renshaw spinal interneurons.

Additional research is needed in order to determine the relative importance of the various mechanisms that might be involved in force perception (sensory feedback from GTOs and efference copy from descending commands and motoneuron activity). One approach might be to use electrical stimulation to create active muscle force and compare the measured force to the subject's perceptions of that force. Electrical stimulation will result in an efference copy signal via antidromic activity in the motor axons and Renshaw collaterals but not in the descending pathways. The model presented here can be used to predict the amount of Ib afferent activity that would be expected as a result of the various unphysiological distributions of active muscle fibers produced by various types and placements of stimulating electrodes.

4.2. Clinical implications of the current observations

The model results presented here allow clinicians to make inferences about the proprioceptive feedback that might be available in patients suffering from certain conditions. The relative loss of motor and proprioceptive feedback varies greatly among stroke and spinal cord injured patients. Even when proprioceptive information is completely cut off from the brain, it can be assumed to contribute to the reflexive activity below the level of the lesion. Our results are particularly interesting for cases where proprioceptive feedback has been spared and FES is used to reanimate the muscles (e.g. in a limb paralyzed by precentral stroke). Such stimulation has also been employed in neurologically intact patients who are unable to exercise muscles adequately as a result of joint pathology (Dupont *et al* 2004). The distorted shape and magnitude of the ensemble GTO activity during electrical stimulation compared to natural recruitment may result in altered perception of muscle force. The GTO activity is also likely to be affected by direct electrical stimulation of afferent axons, depending on the location and intensity of the motor stimulation. FES is usually administered at a fixed pulse rate around 20 pps in order to minimize both tremor and fatigue, which would represent a small but non-negligible fraction of the typical firing rate of an active GTO (typically 100–200 pps; Mileusnic and Loeb 2006).

The modeling results suggest that in patients where reinnervation of the muscle has taken place, the tension information available to the CNS may be little distorted from that available from healthy muscle. This prediction pertains only after several months of recovery, when the muscle fibers have been re-specified by the innervating motor axons (see the previous sections). Additionally, this assumes that the mechanoreceptors are correctly reinnervated and that the regenerated transduction zones have normal properties. Studies suggest, however, that following surgical repair of severed muscle nerves, only a portion of the receptors are reinnervated (30–75%; Banks *et al* 1985, Scott 1991, 1996) and that reinnervation may be by an inappropriate afferent modality (i.e. spindle afferents can innervate GTOs). A recent study where reinnervated muscles failed to generate stretch reflexes suggests caution in interpreting reinnervated proprioceptive feedback. While the encoding of muscle stretch by regenerated individual proprioceptive afferents was remarkably similar to normal, the robust stretch-evoked sensory response that arrived concurrently at the CNS in multiple proprioceptive afferents produced synaptic responses that were either smaller than normal or undetectable (Haftel *et al* 2005). Among many possible mechanisms that might contribute to their observations, the researchers suggest that centrally controlled neural circuits may actively suppress the sensory information encoded by regenerated proprioceptive afferents to prevent the generation of inappropriate stretch reflexes.

Finally, our observations shed light on the utility of microelectrode arrays to record sensory feedback from peripheral nerves or the cell bodies of the primary afferents in the dorsal root ganglion (Branner *et al* 2004, Stein *et al* 2004). One goal of these technologies is to improve the design of neuroprosthetic systems by stimulating the motor axons and also recording signals from skin and muscle sensory fibers to monitor the generated movement. Currently, the stimulation achieved with electrodes implanted at the peripheral nerve (Branner *et al* 2004) is encouraging, but recording sensory activity is more problematic. More promising results were

obtained by implanting the electrode array into the dorsal root ganglia. The recent study showed that recordings from less than ten selected neurons (mostly associated with muscle spindle activity) can accurately predict the limb position while moving the cat's hindlimb passively through a variety of trajectories. In physiologically realistic movement where MUs produce active tensions, however, the GTO afferents will also make significant contributions to the recorded signals. Our ensemble GTO model can provide researchers with predictions about the GTO activity that they can expect during different types of MU recruitment. In particular, it will help to estimate the number of GTO afferents that must be sampled in order to obtain a reliable estimate of muscle force.

5. Conclusions

This study provides evidence in support of the hypothesis that the ensemble rather than individual GTO activity represents a reliable sensor of muscle force. The relationship is predicted to be strong for both normal and reinnervated muscles whose MUs are recruited and frequency modulated according to the size principle. Substantial discrepancies occur when MUs are recruited contrary to the size principle or when either IM or NC stimulation is employed for FES at fixed stimulus rates. Our observations, therefore, emphasize the importance of maintaining size-ordered MU recruitment in the muscle if the CNS is to use the ensemble GTO data as a quantitative feedback signal of muscle tension. Finally, the results of this study can be used in larger models of neural control systems in order to provide better understanding of the actual control problems that must be solved by those systems. Rather than explicitly modeling many individual GTOs and MUs to represent the GTO population in a specific muscle, an estimate of the relationship between the ensemble GTO activity and muscle force can be derived from various simulations presented here.

Appendix A. Calculating the total number of muscle fibers in the cat's MG

The total number of muscle fibers (N_{total}) was obtained by using the whole muscle cross-sectional area (PCSA_{WM}), percentage fiber composition of particular muscle fiber type in the muscle ($\text{percent}_{\text{S}}$, $\text{percent}_{\text{FR}}$, $\text{percent}_{\text{FF}}$) and the cross-sectional area of the particular type muscle fiber (CSA_{S}, CSA_{FR}, CSA_{FF}):

$$\text{PCSA}_{\text{WM}} = \text{percent}_{\text{S}} * N_{\text{total}} * \text{CSA}_{\text{S}} + \text{percent}_{\text{FR}} * N_{\text{total}} * \text{CSA}_{\text{FR}} + \text{percent}_{\text{FF}} * N_{\text{total}} * \text{CSA}_{\text{FF}}.$$

By using the mean values of these parameters that are listed in table 1, the total number of fibers in the MG (N_{total}) was estimated to be 141 180. This number is comparable to the Burke and Tsairis' estimates which were based on small area fiber counts (170 000; Burke and Tsairis 1973).

Appendix B. Calculating the MU innervation ratio

The experimental literature suggests several ways in which the mean number of muscle fibers that belong to a single MU (innervation ratio) can be obtained. The first approach, also called the direct one, uses glycogen depletion where individual MU is continuously stimulated following which glycogen-depleted fibers in the muscle are counted (the MG example: Burke and Tsairis 1973). By slicing the muscle through multiple levels along its length, several areas per each slice are selected and the number of glycogen-depleted fibers is counted in order to estimate the total number of depleted fibers in the muscle. In the case of MG, the estimation of total number of muscle fibers in MU based on few areas can be quite complicated because the fibers are not homogenously spread across the muscle and, moreover, because of the pinnation angle whereby a single fiber can be present in several but not all slices. The additional drawback of the glycogen depletion technique involves the S fibers that rely on aerobic glycolysis, in which case the glycogen depletion achieved by this method is typically incomplete despite prolong stimulation times (Burke and Tsairis 1973). The second approach that researchers utilize in calculating the average innervation ratio is the indirect one. By using this approach, the total number of muscle fibers belonging to a particular type (S, FR or FF) is estimated in the muscle, and then divided by the number of MUs of a particular muscle fiber type in order to obtain the indirect mean innervation ratio of a MU of a particular muscle fiber type. For the purpose of our modeling study, we chose the indirect approach (table 1) because the available experimental data obtained using the direct glycogen approach was inaccurate, especially for the case of S MUs.

Appendix C. Calculating the tendon length at the optimal force

The tendon length $\left(L_0^T\right)$ at the optimal force (F_0) was calculated from the tendon length at maximal passive tension. The tendon length at maximal passive tension was obtained by subtracting the fascicle length at the maximal physiological length ($L^f_{\text{max}} = L^f_0 + 0.7$ cm (Heckman *et al* 1992)); L^f_0 = optimal fascicle length = 2.4 cm (Griffiths 1991); and $L^f_{\text{max}} = 2.4\text{ cm} + 0.7\text{ cm} = 3.1$ cm from the maximal whole muscle length ($L^{WM}_{max} = 12.5$ cm; Goslow *et al* 1973) ($L^T_{\text{max}} = L^{\text{WM}}_{\text{max}} - L^f_{\text{max}} = 12.5\text{ cm} - 3.1\text{ cm} = 9.4$ cm). The passive stress produced by the muscle when stretched to the maximal physiological length is 4 N cm^{-2} (Brown *et al* 1996a), which when normalized by F_0/PCSA (32 N cm^{-2}; Scott *et al* 1996) provides the force in units of F_0 ((4 N cm^{-2})/(32 N cm^{-2}) = 0.125 F_0). The length of the tendon and aponeurosis at force 0.125 F_0 (maximal passive force) was approximated to the value 0.96 L^T_0 (Brown *et al* 1996b). By using this observation, the tendon length at F_0 (L^T_0) was calculated to be 9.8 cm ($L^T_0 = L^T_{\text{max}}/0.96 = 9.4\text{ cm}/0.96 = 9.8$ cm).

Appendix D. The definition of the intramuscular electrode recruitment algorithm

In order to model the IM recruitment in Virtual Muscle, it was necessary to decide on the appropriate recruitment algorithm. As mentioned previously, the IM electrode recruits

the muscle in the manner of nerve branch by branch. Because the nerve branches typically carry nerve fibers innervating all three types of MUs (FF, FR and S), the algorithm attempts to keep the recruitment fraction of each fiber type approximately equal. With the increase in the activation level the algorithm recruits the MU belonging to a muscle fiber type that has least percentage of its fibers recruited, which is calculated as the ratio between the cross-sectional area of all MUs of particular type being recruited and cross-sectional area of all MUs (recruited and nonrecruited) of the particular muscle fiber type. Within a single muscle fiber type, the recruitment of MUs is assumed to be in the order where the largest MUs are recruited prior to the smaller ones. The rationale behind this is based on the assumption that the axon innervating the large MU branches more frequently in the muscle, making it more probable to be in the vicinity of the center of FES than the smaller MU of the same muscle fiber type. Finally, the algorithm assumes that the first MU to be recruited in the muscle is the largest FF, following which the largest FR and the largest S MU are recruited. The reason behind this is also related to the larger probability of the nerve innervating the large MU to be in the branch located close to the site of stimulation than the nerve innervating the smaller MU.

References

Alneas E 1967 Static and dynamic properties of Golgi tendon organs in the anterior tibial and soleus muscles of the cat *Acta Physiol. Scand.* **70** 176–87

Banks R W, Barker D and Brown H 1985 Sensory reinnervation of muscles following nerve section and suture in cats *J. Hand Surg.* **10-B** 340–4

Blair E A and Erlanger J 1933 A comparison of the characteristics of axons through their individual electrical responses *Am. J. Physiol.* **106** 524–70

Boyd I A and Davey M R 1966 The composition of peripheral nerves *Control and Innervation of Skeletal Muscle* ed B L Andrew (Edinburgh: Churchill Livingstone) pp 35–47

Boyd I A and Davey M R 1968 *The Composition of Peripheral Nerves* (Edinburgh: Livingstone)

Branner A, Stein R B, Fernandez E, Aoyagi Y and Norman R A 2004 Long-term stimulation and recording with a penetrating microelectrode array in cat sciatic nerve *IEEE Trans. Biomed. Eng.* **51** 146–57

Brown I E and Loeb G E 1998 Post-activation potentiation—a clue for simplifying models of muscle dynamics *Am. Zool.* **38** 743–54

Brown I E, Liinamaa T L and Loeb G E 1996a Relationship between range of motion, L_0, and passive force in five strap-like muscles of the feline hindlimb *J. Morphol.* **230** 69–77

Brown I E, Scott S H and Loeb G E 1996b Mechanics of feline soleus: II. Design and validation of mathematical model *J. Muscle Res. Cell. Motil.* **17** 221–33

Buller N P, Garnett R and Stephens J A 1978 The use of skin stimulation to produce reversal of motor unit recruitment order during voluntary muscle contraction in man *J. Physiol.* **277** 1P–2P

Burke R E 1981 Motor units: anatomy, physiology and functional organization *Handbook of Physiology: The Nervous System* vol 1 (Bethesda, MD: American Physiology Society) pp 345–422 part 1

Burke R E, Strick P L, Kanda K, Kim C C and Walmsley B 1977 Anatomy of medial gastrocnemius and soleus motor nuclei in cat spinal cord *J. Neurophysiol.* **40** 667–80

Burke R E and Tsairis P 1973 Anatomy and innervation ratios in motor units of cat gastrocnemius *J. Physiol.* **234** 749–65

Cameron T, Richmond F J R and Loeb G E 1998 Effects of regional stimulation using a miniature stimulator implanted in feline posterior biceps femoris *IEEE Trans. Biomed. Eng.* **45** 1036–43

Cheng E J, Brown I E and Loeb G E 2000 Virtual Muscle: a computational approach to understanding the effects of muscle properties on motor control *J. Neurosci. Methods* **101** 117–30

Clark B D, Dacko S M and Cope T C 1993 Cutaneous stimulation fails to alter motor unit recruitment in the decerebrate cat *J. Neurophysiol.* **70** 1433–9

Cope T C and Clark B D 1993 Motor-unit recruitment in self-reinnervated muscle *J. Neurophysiol.* **70** 1787–96

Crago P E, Houk J C and Rymer W Z 1982 Sampling of total muscle force by tendon organs *J. Neurophsyiol.* **47** 1069–83

Datta A K and Stephens J A 1981 The effects of digital nerve stimulation on the firing of motor units in human first dorsal interosseous muscle *J. Physiol.* **318** 501–10

Dupont A C, Bagg S D, Baker L, Creasy J L, Romano C, Romano D, Richmond F J R and Loeb G E 2004 First patients with BION implants for therapeutic electrical stimulation *Neuromodulation* **7** 38–47

Fang Z and Mortimer J T 1991 Selective activation of small motor axons by quasitrapezoidal current pulses *IEEE Trans. Biomed. Eng.* **38** 168–74

Foehring R C, Sypert G W and Munson J B 1986 Properties of self-reinnervated motor units of medial gastrocnemius of cat: I. Long-term reinnervation *J. Neurophysiol.* **55** 931–46

Gandevia S C 1996 Kinesthesia: roles for afferent signals and motor commands *Handbook of Physiology. Exercise: Regulation and Integration of Multiple Systems. Neural Control of Movement* (Bethesda, MD: American Physiology Society) pp 128–72 section 12, part I, chapter 4

Golgi C 1878 Intorno alla distribuzione e terminazione dei nervi nei tendini dell'uomo e di altri vertebrati *Rend. R. Ist Lomb. Sci. Lett.* **B11** 445–53 (Reproduced in Golgi C 1903 *Opera Omnia* vol 1 (Milano: Hoepli) pp 133–42

Golgi C 1880 Sui nervi dei tendini dell'Uomo et di altri vertebrati e di un nuovo organo nervosa terminale muscolo-tendneo *Mem. R. Acad. Sci. Torino* **32** 359–85 Reproduced in Golgi C 1903 *Opera Omnia* vol 1 (Milano: Hoepli) pp 171–98

Gordon T 1988 To what extent can the normal organization of motor unit properties be re-established after muscle reinnervation? *The Current Status of Peripheral Nerve Regeneration* ed T Gordon, R Stein and P A Smith (New York: Alan Liss) pp 275–85

Gordon T and Stein R B 1982 Reorganization of motor-unit properties in reinnervated muscles of the cat *J. Neurophysiol.* **48** 1175–90

Goslow G E, Reinking R M and Stuart D S 1973 The cat step cycle: hind limb joint angles and muscle lengths during unrestrained locomotion *J. Morph* **141** 1–42

Gregory J E 1990 Relations between identified tendon organs and motor units in the medial gastrocnemius muscle of the cat *Exp. Brain Res.* **81** 602–8

Griffiths R I 1991 Shortening of muscle fibers during stretch of the active cat medial gastrocnemius muscle: the role of tendon compliance *J. Physiol.* **436** 219–36

Haftel V K, Bichler E K, Wang Q B, Prather J F, Pinter M J and Cope T C 2005 Central suppression of regenerated proprioceptive afferents *J. Neurosci.* **25** 4733–42

Heckman C J, Weytjens J L F and Loeb G E 1992 Effect of velocity and mechanical history on the forces of motor units in the cat medial gastrocnemius muscle *J. Neurophysiol.* **68** 1503–15

Henneman E and Olson C B 1965 Relations between structure and function in the design of skeletal muscles *J. Neurophysiol.* **28** 581–98

Henneman E, Somjen G and Carpenter D O 1965 Functional significance of cell size in spinal motoneurons *J. Neurophysiol.* **28** 560–80

Hoffer J A, O'Donovan M J, Pratt C A and Loeb G E 1981 Discharge patterns in hindlimb motoneurons during normal cat locomotion *Science* **213** 466–8

Houk J C and Henneman E 1967 Responses of Golgi tendon organs to active contraction of the soleus muscle of the cat *J. Neurophysiol.* **30** 466–81

Jami L 1992 Golgi tendon organs in mammalian skeletal muscle: functional properties and central action *Physiol. Rev.* **72** 623–61

Jarvis J C, Mokrusch T, Kwende M M, Sutherland H and Salmons S 1996 Fast-to-slow transformation in stimulated rat muscle *Muscle Nerve* **19** 1469–75

Jones L A 1986 Perception of force and weight: theory and research *Psychol. Bull.* **100** 29–42

Jones L A and Hunter I W 1982 Force sensation in isometric contractions: a relative force effect *Brain Res* **244** 186–9

Jones L A and Hunter I W 1983 Effect of fatigue on force sensation *Exp. Neurol.* **81** 640–50

Jones L A and Hunter I W 1985 Effect of muscle tendon vibration on the perception of force *Exp. Neurol.* **87** 35–45

Kugelberg E, Edstrom L and Abbruzzese M 1970 Mapping of motor units in experimentally reinnervated rat muscle. Interpretation of histochemical and atrophic fibre patterns in neruogenic lesions *J. Neurol. Neurosurg. Psychiat.* **33** 319–29

Lewis D M 1972 The effect of denervation on the mechanical and electrical responses of fast and slow mammalian muscle *J. Physiol.* **222** 51–75

Loeb G E, Marks W B and Hoffer J A 1987 Cat hindlimb motoneurons during locomotion: IV. Participation in cutaneous reflexes *J. Neurophysiol.* **57** 563–73

Lund J P, Richmond F J R, Touloumis C, Patry Y and Lamarre Y 1978 The distribution of Golgi tendon organs and muscle spindles in messeter and temporalis muscles of the cat *Neuroscience* **3** 259–70

Mileusnic M and Loeb G E 2006 Mathematical models of proprioceptors: II. Structure and function of the Golgi tendon organ *J. Neurophysiol.* **96** 1789–802

Prather J F, Clark B D and Cope T C 2002 Firing rate modulation of motoneurons activated by cutaneous and muscle receptor afferents in the decerebrate cat *J. Neurophysiol.* **88** 1867–79

Proske U 1981 The Golgi tendon organ. Properties of the receptor and reflex action of impulses arising from tendon organ *Int. Rev. Physiol.* **25** 127–71

Reinking R M, Stephens J A and Stuart D G 1975 The tendon organs of cat medial gastrocnemius: significance of motor unit type and size for activation of Ib afferent *J. Physiol.* **250** 491–512

Richmond F J R and Stuart D G 1985 Distribution of sensory receptors in the flexor carpi radialis muscle of the cat *J. Morphol.* **183** 1–13

Scott J J A 1991 Recovery of denervated muscle receptors following treatments to accelerate nerve regeneration *Brain Res.* **563** 195–202

Scott J J A 1996 The functional recovery of muscle proprioceptors after peripheral nerve lesions *J. Peripher. Nerv. Syst.* **1** 19–27

Scott S H, Brown I E and Loeb G E 1996 Mechanics of feline soleus: I. Effect of fascicle length and velocity on force output *J. Muscle Res. Cell Motil* **17** 207–19

Singh K, Richmond F J R and Loeb G E 2000 Recruitment properties of intramuscular and nerve-trunk stimulating electrodes *IEEE Trans. Rehab. Eng.* **8** 276–85

Solomonow M 1984 External control of the neuromuscular system *IEEE Trans. Biomed. Eng.* **31** 752–63

Spector S A, Gardiner P F, Zernicke R F, Roy R R and Edgerton V R 1980 Muscle architecture and force-velocity characteristics of cat soleus and medial gastrocnemius: implications for motor control *J. Neurophysiol.* **44** 951–60

Stein R B, Weber D J, Aoyagi Y, Prochazka A, Wagenaar J B M, Shoham S and Normann R A 2004 Coding of position by simultaneously recording sensory neurons in the cat dorsal root ganglion *J. Physiol.* **560** 883–96

Stevens S S 1962 The surprising simplicity of sensory metrics *Am. Psychol.* **17** 29–39

Swett J E and Eldred E 1960 Distribution and numbers of stretch receptors in medial gastrocnemius and soleus muscles of the cat *Anat. Rec.* **137** 453–60

Warszawski M, Telerman-Toppet N, Durdu J, Graff G L A and Coërs C 1975 The early stages of neuromuscular regeneration after crushing the sciatic nerve in the rat. Electrophysiological and histological study *J. Neurol. Sci.* **24** 21–32